Size and shape control of sub-20 nm patterns fabricated using focused electron beam-induced processing

Sangeetha Hari, Cornelis W. Hagen,* Thomas Verduin, and Pieter Kruit
Delft University of Technology, Department of Imaging Physics, Charged Particle Optics Group, Lorentzweg 1, 2628 CJ Delft, The Netherlands

Abstract. In a first study to analyze the feasibility of electron beam-induced deposition (EBID) for creating certain patterns in advanced lithography, line patterns were fabricated on silicon wafers using EBID. The growth conditions were such that the growth rate is fully determined by the electron flux (the current limited growth regime). It is experimentally verified that different patterning strategies, such as serial versus parallel patterning and single pass patterning versus multiple pass patterning, all lead to the same result in this growth regime. Images of EBID lines, imaged in a scanning electron microscope, were analyzed to determine the position of the lines, the width of the lines, and the linewidth roughness (LWR). The results are that the lines have an average width of 13.7 nm, an average standard deviation of 1.6 nm in the center position of the lines, and an average LWR of 4.5 nm (1σ value). As an example of the capabilities of EBID, a logic-resembling lithography pattern was fabricated. © *2014 Society of Photo-Optical Instrumentation Engineers (SPIE)* [DOI: 10.1117/1.JMM.13.3.033002]

Keywords: electron beam-induced deposition; focused electron beam-induced processing; nanofabrication; line edge roughness; patterning; lithography; e-beam lithography.

Paper 14021P received Feb. 28, 2014; revised manuscript received May 26, 2014; accepted for publication Jun. 5, 2014; published online Jul. 3, 2014.

1 Introduction

To make patterns of lateral size smaller than 20 nm is quite challenging using resist-based electron beam lithography as a result of the straggling of the electron beam in the resist layer during the exposure step and the subsequent development process. This is avoided in focused electron beam-induced processing (FEBIP) where a monolayer of precursor molecules, adsorbed to the substrate surface, is employed. Electron beam exposure of such a monolayer results in the dissociation of the precursor molecules and either the direct deposition of molecule fragments, or the removal of substrate atoms. In the former case, the process is called electron beam-induced deposition (EBID) and in the latter case, in which reactive precursor species are used, the process is called electron beam-induced etching. It is a one-step process requiring no development stage. The spatial resolution is determined largely by the electron beam probe size and the secondary electron (SE) emission area around the primary beam.[1] Simulations, as well as experiments, have demonstrated that deposits even as small as 1 nm can be made on thin membrane substrates and as small as 3 nm on bulk Si substrates (see Sec. 2), as long as the aspect ratio of the deposits is kept low (typically 1). When taller structures are grown, the deposits tend to broaden due to electrons escaping from the sidewalls of the deposits. In the last decade, a number of review papers have appeared on the subject of FEBIP.[2–5]

In this work, we will concentrate on EBID. In practice, EBID is carried out in an electron microscope, usually a scanning electron microscope (SEM) but sometimes also in a scanning transmission electron microscope (STEM). The precursor gas is supplied from a nozzle that is usually positioned at $\sim$50-μm distance from the point where the electron beam hits the substrate to create a local pressure higher than the background pressure. When the primary electron (PE) beam hits the substrate, SEs and backscattered electrons (BSEs) are emitted from the sample surface. All these electrons, PE, SE, and BSE, may interact with the adsorbed precursor molecules causing them to dissociate with different probabilities as given by the energy dependence of the dissociation cross section. The growth rate and the shape of the electron-induced deposit are then determined by the precursor supply rate and the current in the electron beam. Two growth regimes can be distinguished: the precursor-limited regime, in which there are always sufficient electrons available, but not always a precursor molecule to dissociate, and the current-limited regime, in which there is ample supply of precursor molecules such that the growth is fully determined by the beam current. In the precursor-limited regime, the area exposed by the electron beam may become depleted of precursor molecules, and then surface diffusion of precursor molecules starts to play a role in the growth process as well. Several authors have successfully modeled the growth of pillars in this regime, using simulations[6–11] and analytical models.[12] The shape of the deposits and the growth rate in this regime become dependent on the particular writing strategy, as the limited precursor supply will require patterns to be written in multiple passes, with waiting times between passes to allow for precursor replenishment.

Summarizing, the EBID process depends on a multitude of parameters: electron flux (beam current), electron energy, electron exit area of scattered electrons, energy distribution of surface electrons, substrate material, substrate temperature, substrate surface properties, the precursor gas flux, precursor surface diffusion, adsorption/desorption of precursor molecules, electron stimulated desorption, electron-induced

*Address all correspondence to: Cornelis W. Hagen, E-mail: c.w.hagen@tudelft.nl

0091-3286/2014/$25.00 © 2014 SPIE

Downloaded From: http://nanolithography.spiedigitallibrary.org/ on 12/07/2015 Terms of Use: http://spiedigitallibrary.org/ss/TermsOfUse.aspx

dissociation cross section, electron beam-induced heating, and background pressure (residual gases). Usually, many of these parameters are not very well known or vary between experiments and between labs. In the literature, many interesting EBID structures can be found, but the circumstances under which they were made are not well known, and therefore, the results are difficult to reproduce by others. The purpose of this work is to start characterizing the EBID process, as is usually done in electron microscopes, in terms of the relevant parameters, and then learn how to control the parameters such that deposits of prescribed size and shape can be fabricated. In Sec. 2, the state-of-the-art of EBID is presented, and in Sec. 3, new results are discussed on linewidth and line edge roughness (LER) of dense lines and spaces fabricated using EBID with different writing strategies.

2 EBID State-of-the-Art

EBID is as old as electron microscopy. It was a problem rather than something useful. During imaging, hydrocarbons that are always present in microscopes are dissociated by the electron beam and cover the sample with a black layer of carbon soot. It was Christy[13] who was the first to exploit this so-called contamination growth to make insulating Si films. Later Broers et al.[14] came up with the idea to use the electron-beam-dissociated hydrocarbon layer as an etching mask and they were able to produce 8-nm metal lines. At the end of the 20th century, Koops et al.[15] pioneered electron beam dissociation of metal containing precursor gases and mixtures of hydrocarbons, and established EBID as an additive lithography technique. But structures grown using EBID were always of sizes larger than 20 nm, and it was Cividjian et al.[16] who realized that in the initial stage of the growth process structures as small as 2 nm can be fabricated. Van Dorp et al.[17] pushed the spatial resolution limit even further and deposited dots of 0.7-nm diameter on thin carbon membranes in a STEM with a 0.3-nm electron probe. It was then discovered that the placement accuracy of the deposits at the few nanometer scales, was prone to the Poisson statistics of the dissociation process.[18] At a somewhat larger scale, but still sub-10 nm, good control over the deposition process was obtained,[19] as is illustrated in Fig. 1.

The next challenge was to achieve similar spatial resolution in the much more user-friendly SEM. Van Kouwen et al.[20] succeeded in depositing dot arrays on carbon membranes, using methyl-cyclo-penta-dienyl platinum trimethyl ($MeCpPtMe_3$, CAS: 94442-22-5) as a precursor gas, with dots as small as 2.8 nm in diameter. These were imaged in annular dark field (ADF) mode using an STEM detector in the SEM. For applications, however, one had to move away from membrane substrates and use Si wafers instead. But that introduces two difficulties: (i) one can no longer rely on the superb ADF imaging, but has to use SE imaging or BSE imaging and (ii) in addition to the PEs and SEs, the electrons backscattered from the bulk substrate will also contribute to the deposition process. The latter difficulty, fortunately, is not a serious problem when making nanostructures. Assume, for simplicity, that the number of BSEs is equal to the sum of the SEs and PEs, that the BSE exit area has a diameter of typically 1 μm, and that the BSEs are equally effective in dissociating precursor molecules as the SEs and PEs. Then, during the growth of a $5 \times 5 \times 5$ nm^3 deposit, i.e., ~4600 atoms, 4600 atoms are also deposited in the 1-μm diameter circular area, i.e., an area that can contain 7 million atoms in a monolayer. So the concentration of deposited atoms due to the BSEs is really low when growing nanostructures. Van Oven et al.[21] succeeded in depositing 3-nm dense lines and spaces on a bulk Si wafer, and imaged the structures using SE detection (see Fig. 2).

This result was basically obtained by trial and error. To achieve a high spatial resolution, a very small working distance in the SEM was chosen, but the precursor supply nozzle could no longer be inserted between the pole piece of the objective lens and the substrate. Therefore, the nozzle was retracted, and the experiments were done by filling the SEM chamber with precursor gas. So, the precursor gas pressure was rather low, such that the experiments were most likely performed in the precursor-limited regime. When depositing lines consisting of overlapping neighboring pixels and exposing each pixel only once, the growth rate of the resulting lines showed an increase over time (the beam step size between pixels was 0.12 nm compared to a probe size of about 2.6 nm). This is due to a proximity effect that arises when the next pixel is deposited partly on top of the sloped sidewall of the previous deposit, thereby emitting

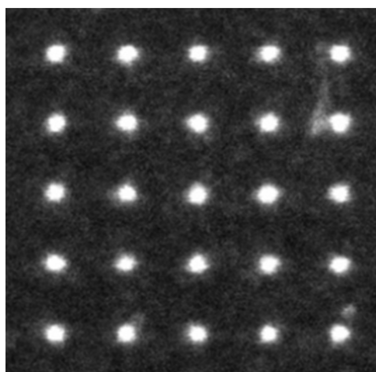

Fig. 1 Annular dark field (ADF) image of an array of 4-nm diameter carbon dots, at 11-nm pitch, deposited on a carbon membrane in a 200 keV scanning transmission electron microscope.

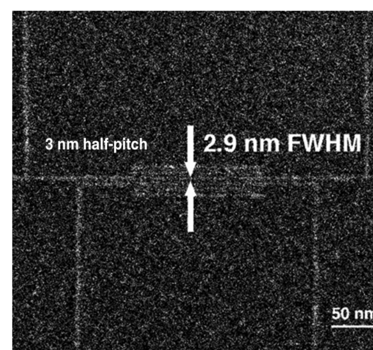

Fig. 2 Secondary electron (SE) image of 3 nm dense lines and spaces deposited in an SEM on a bulk Si wafer, using $MeCpPtMe_3$ as a precursor (30 kV beam, spot 4, 40 ms/nm linear dwell time, 0.96 pC/nm total line dose, beam step size 0.12 nm, 3 mm working distance, 500 passes, synchronized with the power line, and with a 100 ms pause after each pass). [Reprinted with permission from J.C. van Oven et al., *Journal of Vacuum Science & Technology* B29, 06F305 (2011), © 2011, American Vacuum Society.]

Downloaded From: http://nanolithography.spiedigitallibrary.org/ on 12/07/2015 Terms of Use: http://spiedigitallibrary.org/ss/TermsOfUse.aspx

more SEs due to the angular dependence of the SE-yield, and thus dissociating more precursor molecules. A second type of proximity effect occurred when dense lines and spaces were deposited. SEs, emitted from a growing line, dissociate precursor molecules on a previously deposited neighboring line and make it grow further. Both proximity effects could be countered by changing the writing strategy such that the entire pattern is written in multiple passes, keeping the total dose the same. This way, flatter deposits are obtained and neighboring lines are of the same height during the entire growth process. In addition to the proximity problems, the inner area of the dense lines and spaces pattern was observed to become depleted of precursor molecules, evidenced by the fact that less mass was deposited in the inner lines than in the outer lines. This problem could be resolved by inserting a waiting time between passes to allow for replenishment of precursor molecules.

Most EBID structures published in the literature are relatively large structures. Many studies were done on pillars several hundreds of nanometers tall, and the regime in which they were deposited is either the precursor limited regime or is not very well known. In the next section, experiments are described for the deposition of sub-15 nm half-pitch fairly shallow lines, just enough to see the lines in SEM and to determine what dose is required to write recognizable patterns. Also, the patterns will be grown in the current limited regime. It is expected that precursor depletion effects will not occur in this regime, such that waiting times between passes can be avoided. The influence of the writing strategy on the linewidth is investigated, the contribution of the proximity effects is discussed, and a typical EBID pattern of dense lines and spaces will be analyzed in terms of linewidth and linewidth roughness (LWR).

3 Experiment

The deposition experiments were done in a Nova Nano Lab 650 Dual Beam system (FEI Company, Oregon). The precursor gas $MeCpPtMe_3$ was introduced from a nozzle that was located 50 μm above the substrate, close to the point of incidence of the PE beam. The SEM was used in ultrahigh resolution mode with a 20 keV electron beam and a 1.6 nm probe size (spot 2) with a current of 40 pA. The background vacuum of the system was $2.3 \cdot 10^{-6}$ mbar and when the precursor gas was introduced the pressure rose to 1.5 to 2.2×10^{-5} mbar. The substrates used are single side polished p-doped (20 to 30 Ω cm) 525-μm thick silicon wafers. Before patterning, the system, including the substrate, was plasma-cleaned overnight for about 12 h to prevent the codeposition of carbon from contaminants in the microscope. The patterns were defined with FEI patterning software.[22] The beam step size, i.e., the distance between neighboring pixels, was 1 nm. With spot size 2, the overlap between pixels is 38.6%. The microscope is equipped with a fast beam blanker to prevent spurious deposition in between patterns. The shortest dwell time per pixel that could be used reliably was 200 ns. After the deposition, the precursor gas was pumped out of the specimen chamber for at least 1.5 h before the deposits were imaged.

4 Results and Discussion

In resist-based e-beam lithography, it does not matter in what order a pattern is exposed, but in EBID it sometimes does. When writing the pattern in Fig. 2 it was necessary to write the pattern in a parallel order, i.e., in each pass all lines are written and the sequence is repeated multiple times. To prevent local precursor depletion, a waiting time between passes had to be introduced. Writing the same pattern in a serial way, i.e., each line is completed before the next line is deposited, gave a very nonhomogeneous pattern. In the current limited growth regime, there is always an abundant supply of precursor molecules. So, unlike in the precursor limited regime where depletion effects occur, in the current limited regime it should not matter whether a pattern is written in serial or parallel mode and homogeneous deposition is expected. This is used as a test to determine in which regime our experiments are performed. A pattern was designed from the outside going inward consisting of five nested L-shaped lines of single-pixel width, seven nested L-shaped lines of 2-pixels wide, and a 10×10 array of 2 nm $\times$ 2 nm squares. Two of the 2-pixel wide lines are longer than the others to be able to see the difference between isolated lines and dense lines and spaces. In our patterning software,[22] a single-pixel wide line is defined by setting the linewidth to a very small value, in this case 100 pm. The spacing between the lines is 25 nm. The pattern is written from the outside inward with 200 passes and a dwell time per pixel τ_{dwell} of 500 ns. In parallel writing mode, the refresh time, i.e., the time between passes, is 200 ms. The total dose for the lines, defined as the electron beam current delivered in the designed area of 1-pixel (equal to the beam diameter of 1.6 nm) wide, is 250 mC/cm^2, more than 2 orders of magnitude lower than the dose used in Fig. 2. An SEM image of the entire pattern is shown in Fig. 3. The pattern of Fig. 3 was written in parallel and serial writing modes.

Zoomed-in images of the resulting patterns are shown in Fig. 4. The deposition is uniform over the entire pattern in both writing modes, and the isolated lines have the same width as the dense lines, demonstrating that depletion effects are not observed. Therefore, it can safely be assumed that the growth occurred in the current limited regime. The linewidth, as measured from the images, is 7 to 8 nm for the thin lines, and 11 to 12 nm for the thick lines. All lines are wider than the designed width, which means that there is considerable line broadening. The origin of this may lie in surface diffusion of dissociated fragments or precursor dissociation by SEs escaping from the sidewalls of the deposits. Monte Carlo simulations[23] seem to suggest that the latter effect

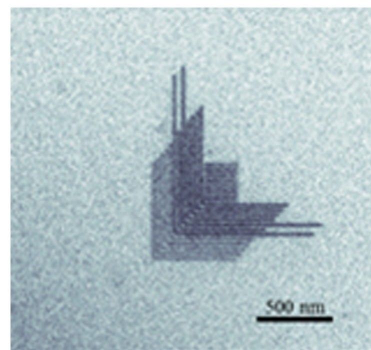

Fig. 3 SE image of a pattern of five single-pixel wide, 12.5 nm half-pitch, L-shaped lines (outer lines), seven 2-pixel wide L-shaped lines (inner lines) at 12.5 nm half-pitch, and a 10×10 array of 2×2 pixel squares. The total dose was 250 mC/cm^2.

Downloaded From: http://nanolithography.spiedigitallibrary.org/ on 12/07/2015 Terms of Use: http://spiedigitallibrary.org/ss/TermsOfUse.aspx

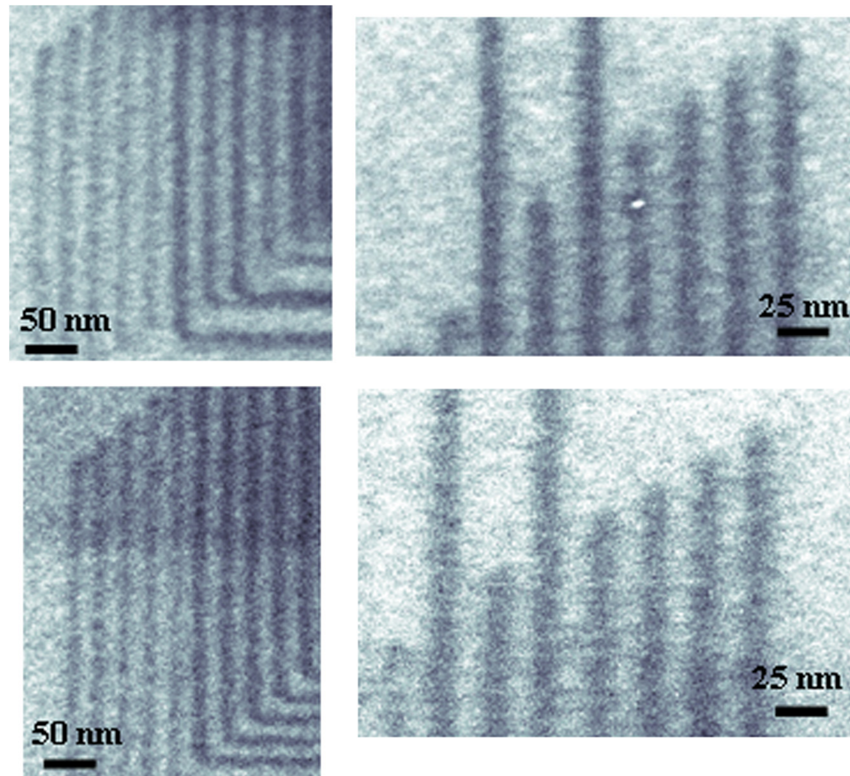

Fig. 4 Zoomed-in SE images of the pattern of Fig. 3. Top images: serial writing mode; bottom images: parallel writing mode; left images: 1-pixel lines (left), 2-pixel lines (right); right images: 2-pixel wide lines. The scale of the bottom images is the same as for the corresponding top image. All lines are at 12.5 nm half-pitch. The total dose was 250 mC/cm^2.

may already occur for quite shallow deposits. This also explains why the 2-pixel wide lines are not twice as wide as the 1-pixel lines; the width is, in fact, largely determined by the broadening. The conclusion from this experiment is that homogeneous deposition is obtained regardless of the writing strategy, suggesting that the experiments were performed in the current limited regime.

In the current limited growth regime, the exposure dose should be the parameter that determines how much mass is deposited and what the size of the deposited pattern will be, irrespective of how the dose is delivered. That is, the dose can be delivered in a single pass exposure with a dwell time per pixel τ_{dwell}, or in N passes with a dwell time per pixel of τ_{dwell}/N, as was done in the previous experiment. This was tested with the following experiment. A pattern was defined of five horizontal parallel single-pixel wide lines at a mutual distance of 30 nm. The patterning strategy is such that the lines were written serially, i.e., one after the other and from bottom to top. The total dose was 500 mC/cm^2. Six patterns were written with $N = 1$, 2, 10, 40, 200, and 800 and $\tau_{\mathrm{dwell}} = 200$, 100, 20, 5, 1, and 0.25 μs, respectively. The deposited lines were imaged in SE imaging mode, and the results are shown in Fig. 5. The image is a collage of the six images stitched together. The left-most image is the single pass result, the right-most image the 800 passes result. Hardly any difference can be seen between lines written with a different number of passes as expected. The spacing between the lines is seen to be 30 nm, and the linewidths are approximately 9 nm. The linewidth is slightly larger than in the previous experiment. This is probably due to the two times larger dose, which causes the lines to broaden more. The single pass line may have shown the proximity effect due to the angular dependence of the SE yield, but this is not observed.

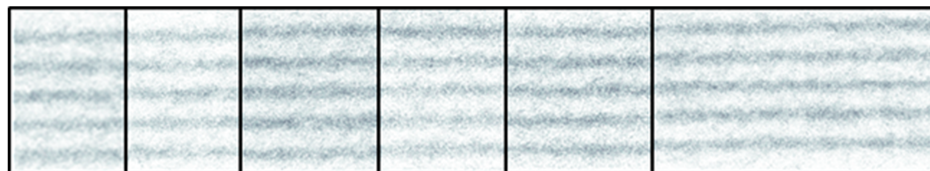

Fig. 5 Six SE images of line patterns stitched together. A pattern was defined of five horizontal parallel single-pixel wide lines at a mutual distance of 30 nm. The patterning strategy is such that the lines were written serially, i.e., one after the other, and from bottom to top. The total dose was 500 mC/cm^2. The six patterns, from left to right, were written with 1, 2, 10, 40, 200, and 800 passes, and dwell times of 200, 100, 20, 5, 1, and 0.25 μs, respectively. For clarity, the contrast of the images was enhanced, but for all images it was done in the same way, to maintain the original intensity differences between images.

Downloaded From: http://nanolithography.spiedigitallibrary.org/ on 12/07/2015 Terms of Use: http://spiedigitallibrary.org/ss/TermsOfUse.aspx

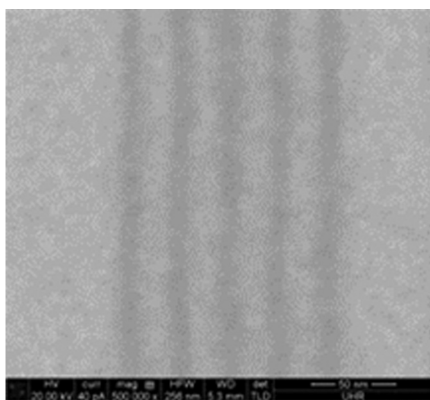

Fig. 6 SE image of five lines deposited at 15 nm half-pitch in serial patterning mode, from left to right. The total dose was 500 mC/cm^2. The pattern was written with 40 passes and a dwell time of 5 μs.

Note that the overlap between neighboring pixels is much smaller (1 nm beam step size) than in the experiment of Fig. 2 (0.12 nm beam step size).

The other proximity effect that enhances the growth of neighboring lines is not observed for the spacing used in these experiments. This is clearly visible in Fig. 4 where the isolated lines have the same width as the dense lines.

What is learned from these experiments is that in the current limited regime it is not required to pattern using multiple passes, but a homogeneous result is obtained even with single pass patterning. This is a good thing, because multiple passes tend to decrease the throughput.

The linewidths mentioned above are only approximate widths as measured from the SEM images. To extract a more meaningful measure for the width of the lines and the LWR, one image of a set of deposited lines was analyzed in more detail. The image is shown in Fig. 6. The writing strategy for this image was the same as for the fourth image from the left in Fig. 5.

To detect the edges of the lines, a recently developed method is used.[24] A brief description is given here. For the details the reader is referred to Ref. 24. First, the image is integrated in the direction of the lines to obtain an integrated line profile (see Fig. 7). This is only an approximation of the line profile because it contains information of the roughness of the lines. If the roughness increases, the profile widens. However, here, this effect is neglected. The signal profile is mirrored with respect to the horizontal axis, and then modeled by matching two vertically shifted Gaussian functions, normalized at the center of the peak. Then the mirrored model function is used to fit each scan line in the image using parameter optimization. The two parameters are the position of the profile and the intensity

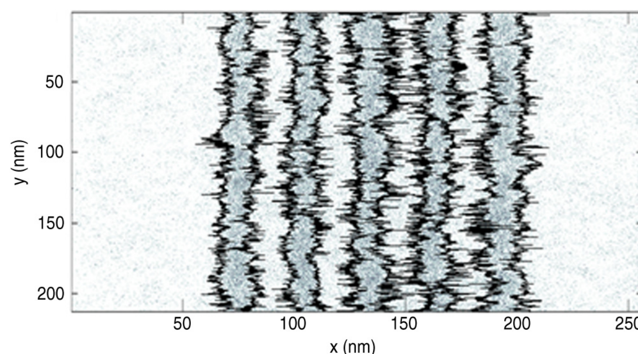

Fig. 8 Contrast enhanced SE image of Fig. 6. The black lines indicate the edges of the lines.

scaling. The result is shown in Fig. 8 where the edges of the lines are plotted, the edge being taken as the position at which the model function is at half-maximum.

The centers of the lines are determined as being halfway between the edges and are plotted in Fig. 9. The mean positions of the lines from left to right are 74.6, 105.7, 134.1, 163.7, and 194.3 nm. The standard deviations are 1.5, 1.6, 1.7, 1.7, and 1.5 nm. The average standard deviation in the center position is 1.6 nm. From the edge positions, the mean linewidths from left to right in Fig. 8 are calculated as: 13.3, 12.0, 14.5, 12.9, and 15.9 nm. The standard deviations are 4.2, 3.8, 5.2, 4.8, and 4.7 nm. The average linewidth is 13.7 nm with an average LWR of 4.5 nm (1σ value). From this, the average LER of the as deposited lines is estimated as 3.2 nm ($\mathrm{LWR}/\sqrt{2}$). It is noted that these standard deviation values are determined for each individual line and also include imaging noise. When averaged over a large number of lines and analyzing the power spectral density,[24] the imaging noise can be largely eliminated and the LWR is expected to be considerably smaller.

The remaining roughness is not due to shot noise in the exposure as a dose of $500\ \mathrm{mC/cm^2}$ corresponds to $31{,}250\ \mathrm{electrons/nm^2}$. It is more likely to be due to the statistical nature of the precursor dissociation process, or surface diffusion of dissociated fragments, or a combination of both. To the best of our knowledge, this is the first time that the LWR and LER have been determined for individual EBID lines, and they are found to be quite large. In particular, the 3σ values are of the order of the linewidth. This poses the challenge of developing methods to decrease the LWR and LER.

As an example of the capabilities of the EBID technique, a pattern is deposited that resembles the typical lithography patterns needed to make logic devices. The result is shown in Fig. 10. The pattern was written exactly as the left-most

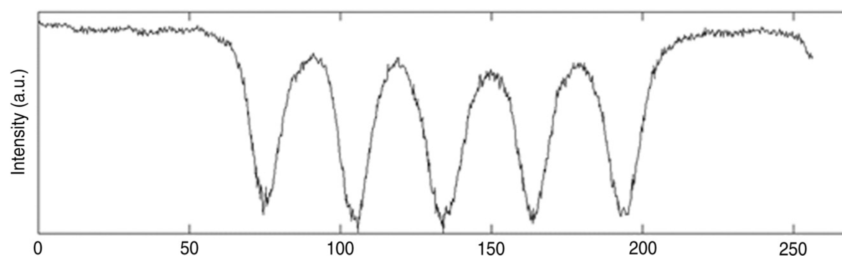

Fig. 7 Integrated line profile of the five lines shown in Fig. 6. The horizontal axis is in nanometer units.

Downloaded From: http://nanolithography.spiedigitallibrary.org/ on 12/07/2015 Terms of Use: http://spiedigitallibrary.org/ss/TermsOfUse.aspx

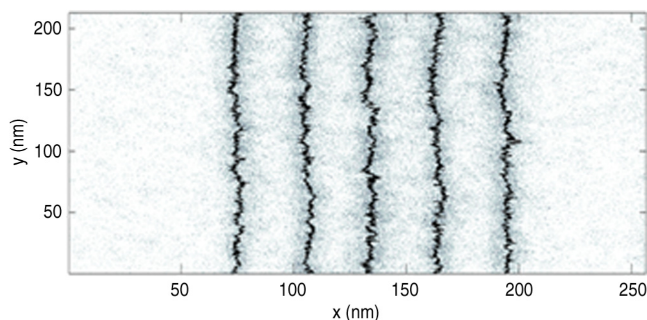

Fig. 9 Contrast enhanced SE image of Fig 6. The black lines indicate the centers of the lines (x-coordinate) along the length of the lines (y-coordinate). The average standard deviation in the center position is 1.6 nm.

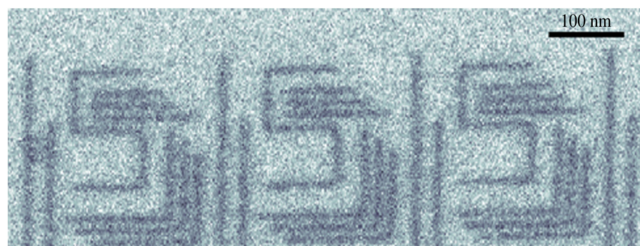

Fig. 10 An example of electron beam-induced deposition pattern consisting of line shapes resembling lithography pattern designs of logic devices. The pattern was written in serial mode, single-pixel wide, single pass, and a dwell time per pixel of 200 μs. The total dose was 500 mC/cm^2. In between writing different lines, the beam was blanked using a fast beam blanker. The linewidths are comparable to the values reported above, i.e., around 10 nm.

pattern of Fig. 5, i.e., in serial mode, single-pixel wide, single pass, and a dwell time per pixel of 200 μs. The total dose was 500 mC/cm^2. In between writing different lines, the beam was blanked using a fast beam blanker. The linewidths are comparable to the values reported above, i.e., around 10 nm. It is to be noted that the EBID technique in principle allows the patterning of any shape, such as squares or circles, as it only requires good control over the electron beam positioning.

5 Conclusions

Experiments were reported on the fabrication of lines using EBID in the current limited growth regime. It was demonstrated that the depletion effects that typically occur when working in the precursor limited growth regime are absent in this regime. Different patterning strategies were compared: parallel versus serial patterning and single pass exposure versus multiple pass exposure. As expected for the current limited growth regime no difference is observed between lines patterned with different writing strategies. This allows for single pass serial exposure, which is preferred over multiple pass parallel exposures for throughput reasons. The proximity effects that were noticed in the previous experiments[21] performed in the precursor limited regime were not noticed here. It must be noted that the line patterns presented here were not at such small spacing as the results in Ref. 21 and shown in Fig. 2. When further decreasing the spacing, the proximity effect that makes neighboring lines grow further may still play a role. This needs to be investigated in the current limited growth regime. A typical set of lines deposited with EBID was analyzed to determine the line position, the linewidth, and the edge roughness. Typical values for the EBID lines are an average width of 13.7 nm, an average standard deviation of 1.6 nm on the center position of the lines, and an average LWR of 4.5 nm (1σ value). As an example of the capabilities of EBID, a logic-resembling lithography pattern was fabricated. A typical dose for these patterns was 500 mC/cm^2. So the challenges are: (i) to reduce the dose, (ii) improve the LWR, and (iii) devise methods to always be in the current limited regime. Also, last but not least, further work has to be done to obtain pure conductors/insulators using EBID.

Acknowledgments

This work is supported by the NanoNextNL, a microtechnology and nanotechnology program of the Dutch Government and 130 partners.

References

1. N. Silvis-Cividjian, C. W. Hagen, and P. Kruit, "Spatial resolution limits in electron-beam-induced deposition," *J. Appl. Phys.* **98**(8), 084905 (2005).
2. N. Silvis-Cividjian and C. W. Hagen, "Electron-beam-induced nanometer-scale deposition," in *Advances in Imaging and Electron Physics*, Vol. 143, pp. 247, Elsevier, San Diego and London (2006).
3. W. F. Van Dorp and C. W. Hagen, "A critical literature review of focused electron beam induced deposition," *J. Appl. Phys.* **104**(8), 081301 (2008).
4. S. J. Randolph, J. D. Fowlkes, and P. D. Rack, "Focused, nanoscale electron-beam-induced deposition and etching," *Crit. Rev. Solid State Mater. Sci.* **31**(3), 55–89 (2006).
5. I. Utke, P. Hoffmann, and J. Melngailis, "Gas-assisted focused electron beam and ion beam processing and fabrication," *J. Vac. Sci. Technol. B* **26**(4), 1197–1276 (2008).
6. J. D. Fowlkes, S. J. Randolph, and P. D. Rack, "Growth and simulation of high-aspect ratio nanopillars by primary and secondary electron-induced deposition," *J. Vac. Sci. Technol. B* **23**(6), 2825–2831 (2005).
7. D. A. Smith, J. D. Fowlkes, and P. D. Rack, "A nanoscale three-dimensional Monte Carlo simulation of electron-beam-induced deposition with gas dynamics," *Nanotechnology* **18**(26), 265308 (2007).
8. K. Rykaczewski, W. B. White, and A. G. Fedorov, "Analysis of electron beam induced deposition (EBID) of residual hydrocarbons in electron microscopy," *J. Appl. Phys.* **101**(5), 054307 (2007).
9. D. A. Smith, J. D. Fowlkes, and P. D. Rack, "Simulating the effects of surface diffusion on electron beam induced deposition via a three-dimensional Monte Carlo simulation," *Nanotechnology* **19**(41), 415704 (2008).
10. D. A. Smith, J. D. Fowlkes, and P. D. Rack, "Understanding the kinetics and nanoscale morphology of electron-beam-induced deposition via a three-dimensional Monte Carlo simulation: the effects of the precursor molecule and the deposited material," *Small* **4**(9), 1382–1389 (2008).
11. J. D. Fowlkes and P. D. Rack, "Fundamental electron-precursor-solid interactions derived from time-dependent electron-beam-induced deposition simulations and experiments," *ACS Nano* **4**(3), 1619–1629 (2010).
12. I. Utke et al., "Resolution in focused electron- and ion-beam induced processing," *J. Vac. Sci. Technol. B* **25**(6), 2219–2223 (2007).
13. R. W. Christy, "Formation of thin polymer films by electron bombardment," *J. Appl. Phys.* **31**(9), 1680–1683 (1960).
14. A. N. Broers et al., "Electron-beam formation of 80-Å metal structures," *Appl. Phys. Lett.* **29**(9), 596–598 (1976).
15. H. W. P. Koops et al., "Characterization and application of materials grown by EBID," *Jpn. J. Appl. Phys.* **33**(12B), 7099–7107 (1994).
16. N. Silvis-Cividjian et al., "The role of secondary electrons in electron-beam-induced-deposition spatial resolution," *Microelectron. Eng.* **61–62**, 693–699 (2002).
17. W. F. Van Dorp et al., "Approaching the resolution limit of nanometer-scale electron beam-induced deposition," *Nano Lett.* **5**(7), 1303–1507 (2005).
18. W. F. Van Dorp et al., "Statistical variation analysis of sub-5-nm-sized electron-beam-induced deposits," *J. Vac. Sci. Technol. B* **24**(2), 618–622 (2006).
19. W. F. Van Dorp, unpublished.
20. L. Van Kouwen, A. Botman, and C. W. Hagen, "Focused electron-beam-induced deposition of 3 nm dots in a scanning electron microscope," *Nano Lett.* **9**(5), 2149–2152 (2009).

Downloaded From: http://nanolithography.spiedigitallibrary.org/ on 12/07/2015 Terms of Use: http://spiedigitallibrary.org/ss/TermsOfUse.aspx

21. J. C. Van Oven et al., "Electron-beam-induced deposition of 3-nm-half-pitch patterns on bulk Si," *J. Vac. Sci. Technol. B* **29**(6), 06F305 (2011).
22. Nano Builder (Version 2.0.0.897), copyright 2013 FEI Company.
23. W. F. Van Dorp et al., "Ultrahigh resolution focused electron beam induced processing: the effect of substrate thickness," *Nanotechnology* **22**(11), 115303 (2011).
24. T. Verduin, P. Kruit, and C. W. Hagen, "Robust determination of line edge roughness in low dose top-down electron microscopy images," *Proc. SPIE* **9050**, 90500L (2014).

Sangeetha Hari is a PhD student at Delft University of Technology. In 2005, she received her Bachelor of Science (honors) degree in physics from University of Delhi, India, followed by a master's degree in physics from the same university in 2007. Then she joined the Tata Institute of Fundamental Research, India (2007 to 2010) to work in experimental molecular physics. Her PhD work, beginning in 2011, is on nanofabrication using electron beam-induced deposition.

Cornelis W. Hagen received a master's degree (1983) and a PhD degree (1991) from the Free University of Amsterdam, The Netherlands. He was a researcher at the Paul Scherrer Institute in Switzerland from 1989 to 1992, and at the Kamerlingh Onnes Laboratory of Leiden University, The Netherlands, from 1992 to 1994. In 1994, he joined Delft University of Technology as an assistant professor and was appointed as an associate professor in 2008. His area of research is microscopy and lithography with charged particles.

Thomas Verduin is a PhD student at Delft University of Technology and specializes in the field of computational physics. In 2009, he received his bachelor's degree in applied physics at Delft University of Technology, The Netherlands. Then he went to Utrecht University to complete a master's study in theoretical physics (2013). In 2012, he started a PhD to investigate shotnoise in e-beam lithography in the charged particle optics group of Delft University of Technology.

Pieter Kruit is a full professor of physics at the Delft University of Technology in the Netherlands. He is (co-)author of over 150 publications in refereed international journals, author of 50 international patents, and supervisor of 30 PhD dissertations. He has had research programs on nanometer-resolution electron spectroscopy, low energy-spread electron and ion sources and multibeam optics for microscopy and lithography. He is cofounder of MAPPER Lithography, a company developing maskless electron beam lithography, and DELMIC.

Downloaded From: http://nanolithography.spiedigitallibrary.org/ on 12/07/2015 Terms of Use: http://spiedigitallibrary.org/ss/TermsOfUse.aspx